

Microscopic model for aging of biocondensates

Hugo Le Roy^{1,*} and Paolo De Los Rios¹

¹*Institute of Physics, École Polytechnique Fédérale de Lausanne—EPFL, 1015 Lausanne, Switzerland*

Biomolecular condensates are membraneless compartments in the cell that are involved in a wide diversity of biological processes. These phase-separated droplets usually exhibit a viscoelastic mechanical response. A behavior rationalized by modeling the complex molecules that make up a condensate as stickers and spacers, which assemble into a network-like structure. The proper functioning of biocondensates requires precise control over their composition, size, and mechanical response. For example, several neurodegenerative diseases are associated with dysfunctional condensates that solidify over a long period of time (days) until they become solid. A phenomenon usually described as aging. The emergence of such a long timescale of evolution from microscopic events, as well as the associated microscopic reorganization leading to aging, remains mostly an open question. In this article, we explore the connection between the mechanical properties of the condensates and their microscopic structure. We propose a minimal model for the dynamic of stickers and spacers, and show that entropy minimization of spacers leads to an attractive force between stickers. Our system displays a surprisingly slow relaxation toward equilibrium, reminiscent of glassy systems and consistent with the liquid-to-solid transition observed. To explain this behavior, we study the clustering dynamic of stickers and successfully explain the origin of glassy relaxation.

INTRODUCTION

Liquid-liquid phase separation has emerged as a major organizing principle for the compartmentalization of cellular processes into membraneless organelles known as biomolecular condensates. Condensates are associated with various functions of the cell, although their precise role often remains elusive [1], to the point that it is not even clear if some of them are functional, incidental or pathological [2]. Similarly, little is known about the complete composition of condensates; however, one or several scaffolding components that drive the phase separation can usually be identified, including proteins, DNA [3, 4], or RNA [5, 6]. Despite their diversity, condensates also display common features. It is usually accepted that their formation requires weak multivalent interactions [7], mediated by disordered portions of proteins [8] or by RNA/DNA-protein interactions [9]. Similarly, micro-rheology experiments suggest that biocondensates exhibit a general viscoelastic mechanical response [10, 11]. This picture has been rationalized through the sticker and spacer model, which describes proteins as generic sequences of sticky (stickers) and non-sticky (spacers) regions [12]. The complex interactions that make up a condensate give rise to an emergent long-time transition to a solid-like state, usually described as aging [13, 14]. This process has been associated with protein denaturation [15], amyloid formation [16] and, from a physiological perspective, with neurodegenerative diseases [17]. Current physical pictures of condensate aging either rely on the modeling of specific proteins' interaction – like β -sheet stacking [18] –, or do not model the microscopic dynamic of the components [19, 20]. Yet, aging seems to be a fairly general behavior, essentially insensitive to the details of the condensate's composition, which

suggests that a universal physical mechanism may govern this transition. A general microscopic picture explaining how large timescales (days or more) emerge from a collection of microscopic processes, that typically occurs on much shorter timescales, (μs) is missing.

In this work, we use the sticker and spacer framework to model the microscopic structural rearrangement taking place in condensates, and leading to aging. This approach essentially considers proteins as a heterogeneous collection of localized, attractive regions (stickers) and longer, neutral regions (spacers). Stickers reversibly associate via non-covalent interactions, while spacers provide flexibility and connection between stickers, resulting in the formation of a percolating network. The ensuing mechanical behavior of this network is typical of an associative gel, characterized by a viscoelastic response to stress. At short timescales, the gel displays solid, elastic-like behavior due to the entropic elasticity of the spacers, resisting deformation. Conversely, over longer timescales, the reversible binding and unbinding of stickers enable the material to flow, displaying liquid-like characteristics. Homogeneous associative gels display a soft relaxation over a single characteristic timescale, directly related to the unbinding dynamics of the stickers [21]. In contrast, heterogeneous gels feature multiple coexisting timescales, each corresponding to a different sub-region within the system, and a complex relaxation behavior emerges from their superposition [22]. Strong heterogeneity results in a broad distribution of timescales, sometime heavy tailed. In these extreme cases, a portion of these timescales are arbitrarily large and relaxation seemingly never ends, a phenomena typical of glasses, and known as aging [23, 24]. To investigate how aging can emerge from the collective rearrangement of the gel components, we model them as sticker and spacer. the former acting as diffusing particles that can bind to (and unbind from) the latter, that represent Gaussian polymers, possibly capturing intrinsically disordered regions of proteins or long

* h.leroy@epfl.ch

RNA strands. Using a combination of analytical results and simulations, we show that an entropic Casimir-like force drives the clustering of stickers, in accordance with several other works [3, 15, 25]. We find that collective rearrangement of the stickers induce a slow-down of the dynamic of the system. As a consequence, the relaxation toward equilibrium is surprisingly slow and reminiscent of the usual glass dynamic [26]. To explain our observations, we introduce a minimal model for the dynamic of clusters, which provide a scaling law for the dynamical slowing-down. Despite its simplicity, our model displays a rich phenomenology leading to glassy dynamic which includes emergence of large timescales, ergodicity breaking and aging. By focusing on the minimal ingredients required for the emergence of a soft glassy relaxation, our model proposes a universal mechanism to aging of complex associative gels.

RESULTS

Dynamic of stickers and spacers

We first introduce a physical model for the dynamic of stickers and spacers. Starting with spacers, which correspond to RNA or DNA strands, or to intrinsically disordered segments of proteins. Their dynamics are similar to those of a polymer, and we consider the dilute regime where excluded volume or topological constraints due to entanglement are negligible. Therefore, we model spacers as linear Gaussian polymers. In this work, we will focus on the dynamic of a single polymer strand and treat the others effectively. To model protein interactions, we consider that polymers interact with a background disordered potential, effectively representing the surrounding environment as represented in Fig. 1. The positions of the minima of this potential correspond to the positions of the stickers. We propose that the long time evolution of the condensates results from the slow evolution of the background potential, that we model through the diffusion of stickers. While the diffusion dynamics of stickers may differ from a free particle depending on the exact nature of what they represent, we expect that the details of the microscopic dynamics will not significantly affect the long-time evolution of our system. Additionally, considering that stickers correspond to proteins or sticky regions of a protein, we treat them as effectively always bound to another polymer strand in the background. As a consequence, whenever the polymer binds to a sticker, it effectively creates a cross-link that impairs its diffusion and constraints the conformations of the polymer. Here, we consider the limiting case where stickers do not diffuse at all when bound to the polymer, thus creating an anchoring point. This dynamic provides enough freedom for the system to rearrange while capturing the constraining effect of binding.

To describe the dynamic of the stickers, we now consider the probability of the i -th sticker to be in position

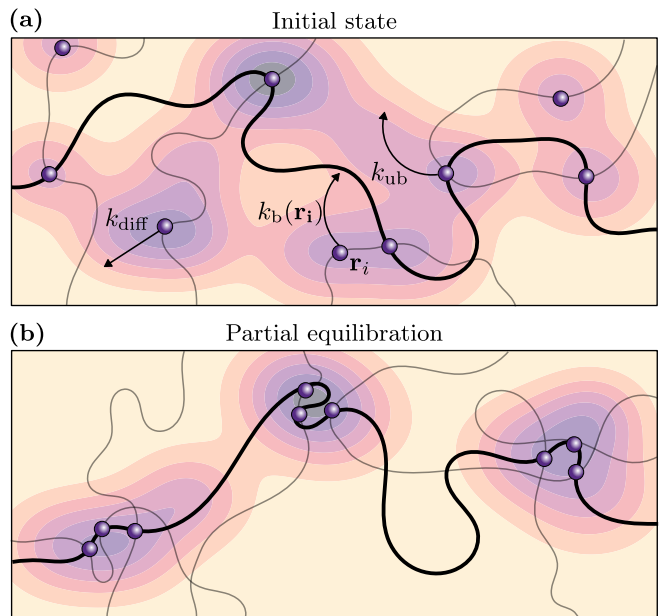


FIG. 1. Schematic representation of our sticker and spacer model. The disordered background potential is represented as a color coding, while stickers are represented as diffusing particles. We focus on a single polymer dynamic highlighted in bold, while the other effective polymers are in shaded. (a) Represents the initial state in which stickers are homogeneously spread in space. (b) Qualitatively represent a typical final state as predicted by our model.

\mathbf{r}_i at time t in the bound state along the lineic position ℓ of the polymer denoted by $p_b(\mathbf{r}_i, \ell, t)$. Similarly, we write the probability to be unbound $p_{ub}(\mathbf{r}_i, t)$. Given the previously introduced dynamics, the time evolution of these two probability distributions is governed by the two coupled master equations:

$$\begin{aligned} \partial_t p_b(\mathbf{r}_i, \ell, t) &= k_b(\mathbf{r}_i, \ell) p_{ub}(\mathbf{r}_i, t) - k_{ub} p_b(\mathbf{r}_i, \ell, t) \\ \partial_t p_{ub}(\mathbf{r}, t) &= k_{ub} p_b(\mathbf{r}_i, \ell, t) - k_b(\mathbf{r}_i, \ell) p_{ub}(\mathbf{r}_i, t) + D \nabla^2 p_{ub}(\mathbf{r}_i, t), \end{aligned} \quad (1)$$

where k_b and k_{ub} are respectively the binding and unbinding rates of the sticker with the considered polymer. We first write the unbinding rate using a single energy scale under the Kramers approximation:

$$k_{ub} = \frac{1}{\tau_0} e^{-\beta E_b}, \quad (2)$$

where $\beta = 1/(k_B T)$ is the inverse temperature, E_b the binding energy scale, and τ_0 a timescale associated with the microscopic escape process. While the complexity of real proteins' interaction should lead to a distribution of binding energies, we show here that this assumption is not necessary for the system to display a glassy dynamic, and address the effect of a more complex model in the discussion section.

Concerning the binding rate, we assume that the disordered potential represented by the stickers is partially-quenched. Meaning that it evolves on a much larger

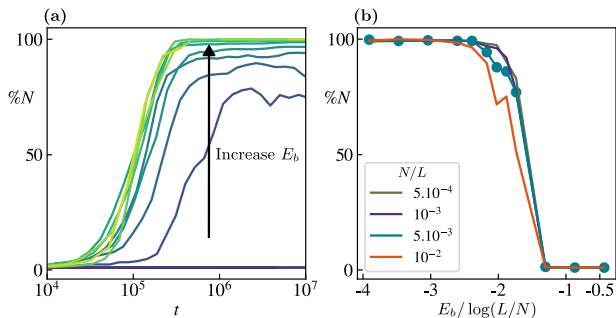


FIG. 2. **(a)** Early time evolution of the Percentage of bound stickers in the system. Here, we use $L = 2.10^4$ and $N = 100$. **(b)** Plateau value of the percentage of bound stickers as a function of the binding energy, rescaled by the lineic density of stickers. The scattered points correspond to the measurements obtained from the panel **(b)**.

timescale than the polymers. As a consequence, polymers have time to equilibrate between two binding/unbinding events. Assuming that all conformations of the polymer are equiprobable, we show in Supplementary Material that the probability for a given conformation of the polymer to meet a sticker located at \mathbf{r} in a volume a^3 (where a is the monomer size) at a lineic position ℓ is given by:

$$p_{\text{meet}}(\mathbf{r}, \ell) = e^{S_{\text{b}}(\mathbf{r}, \ell) - S_{\text{ub}}}. \quad (3)$$

where S_{b} and S_{ub} correspond to the entropy of the polymer strand when bound and unbound to the sticker, respectively. Our approximation of fast polymer conformational exploration means that the limiting timescale is the binding time. Thus, we write the binding rate of the sticker to the polymer as:

$$k_{\text{b}}(\mathbf{r}, \ell) = 1/\tau_0 \sum_{\alpha} p_{\text{meet}}^{\alpha}(\mathbf{r}, \ell) = 1/\tau_0 \sum_{\alpha} e^{S_{\text{b}}^{\alpha}(\mathbf{r}, \ell) - S_{\text{ub}}^{\alpha}}, \quad (4)$$

Where the sum over α represents the participation of all the polymer strands in the vicinity of the given sticker. Together with (2), this expression respects detailed balance, thus guaranteeing that the evolution of the system is consistent with thermodynamic equilibrium. Notice that $S_{\text{b}}^{\alpha}(\mathbf{r}, \ell)$ introduces a coupling between the dynamic of the different stickers through ℓ that ultimately depends on where all the other stickers are bound (see Supplementary Material for the full expression). As a result, we cannot directly solve this system of equation without further approximation. In the next section, we use a Gillespie simulation to study the time evolution of our system.

Early time behavior

We simulate a polymer of length L , which defines the system size, surrounded by N initially unbound stickers spread homogeneously in space. First, looking at

the early time evolution of the system, we observe in Fig. 2 **(a)** a rapid increase in the number of stickers bound to the polymer until a plateau is reached. We show in Fig. 2 **(b)** how the height of the plateau depends on the binding energy, observing a sharp increase from 0% of the bound stickers to 100% at a critical value of the binding energy. This phenomenon is reminiscent of the phase transition observed in the Poland-Scheraga model of DNA denaturation [27]. In their model, two DNA strands can bind to one another through sticky base pairs that are regularly spaced along the strands. Similarly to our model, the energetic binding energy must overcome the loss of entropy associated with the binding. As the linear density of stickers increases, it becomes increasingly favorable to bind them as the entropic cost for successive binding decreases. Their theory predicts a phase transition with a critical energy scaling, $E_c \propto \log(L/N)$. We observe that our model consistently displays a similar scaling based on the collapsed curves of Fig.2 As a consequence, for our system, low values of the binding energy (or high temperature) mean that stickers are mostly unbound, and the system mechanically responds like a liquid. If the value of the binding energy is higher than its critical value (or the temperature lower than its critical value), stickers remain bound most of the time, leading to a viscoelastic mechanical response similar to that of an associative gel. This type of gel displays a solid-like mechanical response at timescales lower than the unbinding time and liquid-like at timescales much larger than the unbinding time. In this work, we focus on the viscoelastic aging regime; for this reason, we always consider the binding energy above its critical value. In this case, unbinding becomes the time-limiting process for the dynamics of the system. In the following, we do not discuss the influence of the binding energy, which can be ruled out by rescaling times with respect to $1/k_{\text{ub}}$. In the high energy regime, the phenomena discussed are insensitive to the value of the binding energy.

Glassy relaxation

Once all stickers are bound, the system's energy becomes essentially fixed. However, the entropy of the polymer also depends on the positions of the stickers. We study the equilibration of the system through the diffusion of stickers. By setting the time derivative of the master equation to zero and independently equilibrating the binding/unbinding dynamics and the diffusion dynamics, we demonstrate in the Supplementary Material that the equilibrium probability distribution of finding two stickers interacting with a polymer of length L at a distance $|r|$ from each other is given by:

$$p(r) = \frac{3\text{erfc}\left(\sqrt{\frac{3}{2aL}}|r|\right)}{2\pi aL|r|} \quad (5)$$

We derive an approximated formula in Supplementary

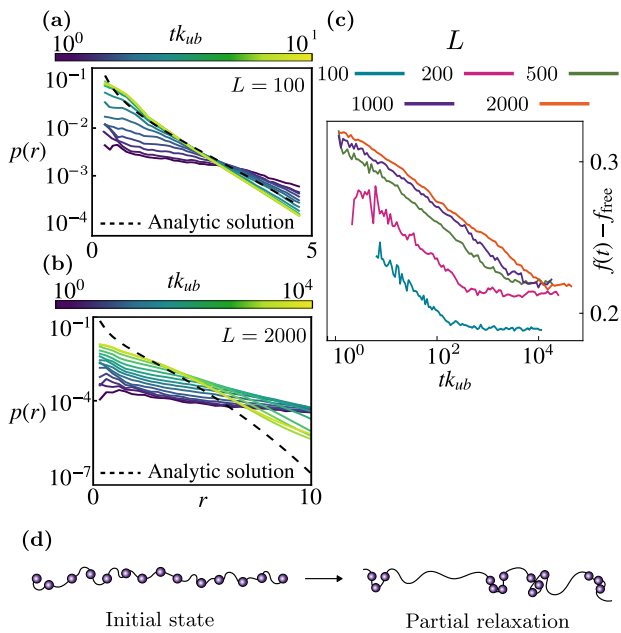


FIG. 3. **(a)** sticker distance probability distribution at different time-point. The color coding corresponds to the time, and the analytical solution is provided as dotted line. We simulate systems with fixed lineic density: $N/L = 5 \cdot 10^{-2}$. Small systems of length $L = 100$ successfully converge toward the equilibrium distribution. Whereas, large systems, of length $L = 2000$, evolves toward the analytic solution without reaching it. **(b)** We follow the equilibration process by looking at the decay of the free energy per unit length over time, the initial binding regime as been removed for improved visibility. Using a fixed lineic density of stickers, we expect all curves to converge to the same relative value. Large systems are stuck at a higher value of the free energy, stressing its inability to reach equilibrium.

Material for a system of N particles, considering polymer strands that mediate interactions as a mean field. The simulated time evolution of the probability distribution toward the expected equilibrium analytic solution for smaller systems is depicted in Fig. 3 (a). Contrastingly, Fig. 3 (b) shows that larger systems, while converging similarly, do not reach the predicted equilibrium solution. To further characterize the relaxation of our system toward equilibrium, we plot, in Fig. 3 (c), the free energy per unit length difference between our system and the theoretical free energy of an unconstrained polymer. Calculated as $f_{free} = F_{free}/L = NE_b/L - \log(4\pi)$ (where 4π is the solid angle between two monomers). We use a fixed lineic density of stickers ($N/L = 5 \cdot 10^{-2}$) and different system sizes, characterized by L . We observe a slow logarithmic decay of the free energy, followed by a plateau, where the total relaxation time depends on the system size. This type of logarithmic relaxation is usually associated with glassy systems [26], and we propose a model in the next section to better understand this unique behavior. Looking at the height of the plateau, we notice that it first increases with the system size be-

fore becoming independent of it. This is an unexpected behavior as the system is self-similar along the polymer, and the equilibrium free energy per unit length is an intensive quantity with respect to L . Additionally, we show in Supplementary Material that the height of the plateau also depends on the diffusion constant, k_{diff} . These results suggest that systems above a certain size are unable to fully relax to equilibrium. Instead, they form substructures, each equilibrated, that we call clusters. We propose in Fig. 3 (d) a 1D schematic of this picture. Starting from a homogeneous distribution of stickers, they aggregate into equilibrated clusters. If the total system size is similar to the typical cluster size, the plateau free energy is the equilibrium one. For a system much larger than the cluster size, the plateau free energy is higher in average and intensive again.

To further examine the formation of equilibrated subsystems, we employ a hierarchical clustering algorithm to group stickers into clusters. This algorithm uses a single maximum length to define connectivity, here, we use the characteristic lengthscale of Eq. (5) to match the definition of clusters as equilibrated subsystems. Fig. 4 (a) illustrates the time evolution of the relative cluster size, showing that smaller systems tend to converge into a single cluster, while larger systems form clusters of fixed size, effectively showing a decay in the relative size.

Origin of the glassy relaxation

We now investigate the origin of the slow logarithmic relaxation dynamics of the free energy. Logarithmic decay typically implies a continuous slowing down of the dynamics during relaxation. To confirm this, we examine the intermediate scattering function (ISF), defined as:

$$I(\mathbf{k}, t) = \sum_{j=0}^N \left\langle e^{i\mathbf{k}(\mathbf{r}_i(t) - \mathbf{r}_j(0))} \right\rangle. \quad (6)$$

The modulus of the ISF characterizes the spatial and temporal dependence of the relaxation dynamics, It is commonly used to study glassy relaxations [28]. Here, we focus on the wave vector associated with the inter-sticker distance, $k = 1/\langle r \rangle$, where $\langle r \rangle$ is the average sticker distance computed from Eq. (5). In Fig. 4 (b), we plot the decay of the ISF over time, quantifying the decorrelation of the stickers' positions after a lag time denoted t_{lag} along the relaxation. Unlike an exponential decay consistent with a normal random walk, we observe a stretched exponential relaxation defined by $\exp((-t/\tau)^\alpha)$, with $\alpha \approx 0.7$. This stretched exponential decay is characteristic of the α relaxation in glassy liquids [29, 30] and indicates a relaxation slower than exponential, usually associated with subdiffusive microscopic processes [31]. By fitting the measured ISF with a stretched exponential, we extract the characteristic relaxation time of the system. The inset of Fig. 4 (b) shows

the increase of the characteristic relaxation time τ as a function of the simulation time, confirming our intuition of a dynamical slow-down.

We now propose a model for the origin of this dynamical slow-down. In the previous section, we demonstrated that system equilibration involves the growth of clusters. Individual exchanges of stickers between clusters do not modify the average size; to increase the average cluster size, it is necessary to dissolve another cluster. To compute the dissolution time of a cluster, we consider a system with N stickers spread across clusters. The average number of stickers in a cluster is denoted \bar{n} . We model the exchange of stickers as a two-step process: unbinding from one cluster and then rebinding in a random cluster, selected randomly and with equal probability from all available clusters. Each exchange occurs according to a Poisson process with a constant rate $1/\tau_{\text{exch}}$, which effectively encapsulates a complex process of diffusion coupled to the binding/unbinding dynamic, that we do not investigate here. For a given cluster, the probability $P(n, t)$ to contain n stickers at time t evolves as:

$$\frac{dP(n, t)}{dt} = 1/\tau_{\text{exch}} [P(n+1, t)(n+1) + P(n-1, t)\bar{n} - P(n, t)(n+\bar{n})], \quad (7)$$

derived from the master equation, where a cluster with n stickers loses one at a rate $1/\tau_{\text{exch}}n$ and gains one from any of the N/\bar{n} clusters at a rate $N/(N/\bar{n})/\tau_{\text{exch}} = \bar{n}/\tau_{\text{exch}}$. Assuming that the smallest cluster is the one dissolving first, and $N \rightarrow \infty$, we compute in the Supplementary Material the average dissolution time:

$$\tau(\bar{n}) \underset{N \rightarrow \infty}{\sim} \tau_{\text{exch}} \frac{e^{\bar{n}}}{\bar{n}^2}, \quad (8)$$

We now investigate the long-time collective growth of clusters resulting from the dissolution of other clusters. Assuming that clusters dissolve at a rate $1/\tau(\bar{n})$, and its sticker is redistributed among the $N/\bar{n} - 1$ other clusters. We describe the dissolution events as continuous in time, and write a differential equation for the time evolution of the average cluster size:

$$\frac{d\bar{n}}{dt} = 1/\tau_{\text{exch}} e^{-\bar{n}} \frac{\bar{n}^2}{N/\bar{n} - 1}, \quad (9)$$

This non-linear differential equation cannot be solved analytically; however, we show in the Supplementary Material that for a large systems (N and \bar{n} large) $\bar{n} \propto \log(t)$. This logarithmic scaling can be used together with the dominant factor of Eq. (8): $\tau(\bar{n}) \propto e^{\bar{n}}$. Which gives $\tau(t) \propto t^\gamma$, where γ is a constant that depends on τ_{exch} . This power-law qualitatively agrees with the inset of Fig. 4 (b), which confirms the relation between the relaxation time of the ISF, and the dissolution time of growing clusters. Here, we focused on the dominant mathematical factors, and neglected many processes that could provide a more quantitative agreement with the simulation. This

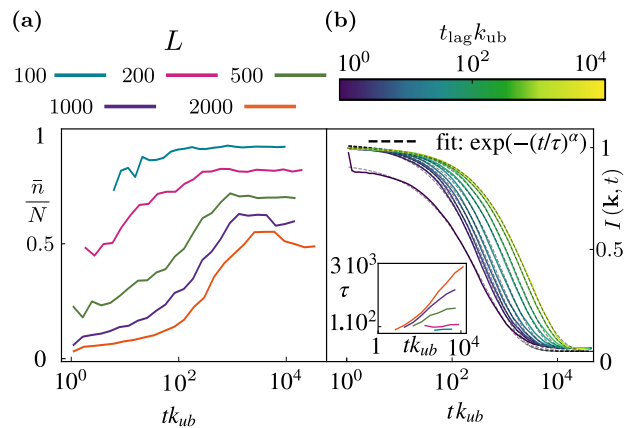


FIG. 4. (a) average cluster size evolution, clusters are built using a hierarchical algorithm that use a minimum distance linkage criteria. The distance used is the average sticker distance computed using the pair correlation function of Eq. (5), in our case $\bar{d} = 3.6$. (b) Modulus, of the intermediate scattering function for $|\mathbf{k}| = 1/\bar{r} = 0.37$, where \bar{r} is the average distance between stickers. The stretched exponential fits are in good agreement, and the corresponding τ values obtained are plotted in the inset. The value of α does not evolve significantly over time, and remains ≈ 0.7 .

choice is motivated by the initial strong simplification of our sticker and spacer model. And we believe that only qualitative results will be robust to the addition of real microscopic details.

DISCUSSION

We have introduced a minimal model to describe the dynamics of protein or RNA/DNA-protein condensates. By utilizing the general sticker and spacer framework, we examined the long-term structural evolution of these systems. Our investigation primarily focused on two general effects: the entropic cost associated with binding and the increasing difficulty of the system to rearrange upon equilibration. Our model reveals two distinct mechanisms: the emergence of a Casimir attractive force between stickers mediated by spacers and the clustering of stickers leading to glassy relaxation. The first mechanism is reminiscent of bridging-induced phase separation, where RNA or DNA-protein binding is driven by a similar entropic force, triggering condensation [3, 9]. In our framework, this entropic attractive force appears for high binding energy, as the simultaneous unbinding of multiple stickers would disrupt the attractive interaction. This approximation might not be universally valid for all biological systems. In fact, we anticipate that in many cases, the Casimir force will not be the primary driver of structural reorganization. Nonetheless, in our model, this attractive force is only useful to drive sticker clustering, which is ultimately responsible for glassy relaxation. This clustering can also be driven by system-specific mechanisms,

such as three-body stabilizing interactions or multiple β -sheet stacking, and has been observed in experimental systems [15, 25, 32]. In fact, such clustering is also a general behavior of random walkers in disordered media, commonly known as localization in this context [33]. For these reasons, we are confident that the clustering of stickers described here is a fairly universal feature, from which we have only highlighted the entropic minimization effect.

Our model shares similarities with previously studied models of random walker with trap [34, 35], which reproduce key features, such as glass transition, subdiffusion, or localization, reminiscent of the phenomenology observed here. However, these models use a prior distribution of binding energies (e.g., exponential), aging occurs through the exploration of deeper and deeper traps by the random walker. On the one hand, real proteins exhibit a distribution of interaction energy, which is sufficient to induce complex relaxation of a single protein [36]. On the other hand, proteins' interactions –electrostatic,

hydrophobic, or hydrogen bonding– are all of the same order of magnitude ($\approx 10k_B T$), which should lead to a fairly narrow distribution of interaction energy. For this reason, intrinsic protein complexity does not justify *a priori* the existence of ever-deepening traps needed for long-time aging. Our model offers a rationale for considering a broad distribution of energetic interactions, as proposed in previous studies [19, 37]. By focusing on the exponential part of Eq. (8), we find that the dissolution time of clusters is similar to a Kramer escape time for a trap of depth \bar{n} time larger than an isolated sticker. Such mechanism is known for enhancing small heterogeneities of stickers, leading to complex viscoelastic relaxation [38].

ACKNOWLEDGMENTS

We thank Lara Koehler for her critical reading of the manuscript. This work was supported by the Swiss National Science Foundation under grant CRSII5 193740.

-
- [1] S. F. Banani, H. O. Lee, A. A. Hyman, and M. K. Rosen, Biomolecular condensates: Organizers of cellular biochemistry, *Nat Rev Mol Cell Biol* **18**, 285 (2017).
- [2] Y. Shin and C. P. Brangwynne, Liquid phase condensation in cell physiology and disease, *Science* **357**, eaaf4382 (2017).
- [3] J.-K. Ryu, C. Bouchoux, H. W. Liu, E. Kim, M. Minamino, R. de Groot, A. J. Katan, A. Bonato, D. Marenduzzo, D. Michieletto, F. Uhlmann, and C. Dekker, Bridging-induced phase separation induced by cohesin SMC protein complexes, *Sci Adv* **7**, eabe5905 (2021).
- [4] K. Rippe, Liquid–Liquid Phase Separation in Chromatin, *Cold Spring Harb Perspect Biol* **14**, a040683 (2022).
- [5] M. Hondele, R. Sachdev, S. Heinrich, J. Wang, P. Valotton, B. M. A. Fontoura, and K. Weis, DEAD-box ATPases are global regulators of phase-separated organelles, *Nature* **573**, 144 (2019).
- [6] A. Aulas, M. M. Fay, S. M. Lyons, C. A. Achorn, N. Kedersha, P. Anderson, and P. Ivanov, Stress-specific differences in assembly and composition of stress granules and related foci, *Journal of Cell Science* **130**, 927 (2017).
- [7] C.-Y. S. Lee, A. Putnam, T. Lu, S. He, J. P. T. Ouyang, and G. Seydoux, Recruitment of mRNAs to P granules by condensation with intrinsically-disordered proteins, *eLife* **9**, e52896 (2020).
- [8] S. Boeynaems, S. Alberti, N. L. Fawzi, T. Mittag, M. Polymenidou, F. Rousseau, J. Schymkowitz, J. Shorter, B. Wolozin, L. V. D. Bosch, P. Tompa, and M. Fuxreiter, Protein Phase Separation: A New Phase in Cell Biology, *Trends in Cell Biology* **28**, 420 (2018).
- [9] C. A. Brackley, S. Taylor, A. Papantonis, P. R. Cook, and D. Marenduzzo, Nonspecific bridging-induced attraction drives clustering of DNA-binding proteins and genome organization, *Proceedings of the National Academy of Sciences* **110**, E3605 (2013).
- [10] L. M. Jawerth, M. Ijavi, M. Ruer, S. Saha, M. Jahnelt, A. A. Hyman, F. Jülicher, and E. Fischer-Friedrich, Salt-Dependent Rheology and Surface Tension of Protein Condensates Using Optical Traps, *Phys. Rev. Lett.* **121**, 258101 (2018).
- [11] I. Alshareedah, M. M. Moosa, M. Pham, D. A. Potoyan, and P. R. Banerjee, Programmable viscoelasticity in protein-RNA condensates with disordered sticker-spacer polypeptides, *Nat Commun* **12**, 6620 (2021).
- [12] J.-M. Choi, A. S. Holehouse, and R. V. Pappu, Physical Principles Underlying the Complex Biology of Intracellular Phase Transitions, *Annual Review of Biophysics* **49**, 107 (2020).
- [13] L. Jawerth, E. Fischer-Friedrich, S. Saha, J. Wang, T. Franzmann, X. Zhang, J. Sachweh, M. Ruer, M. Ijavi, S. Saha, J. Mahamid, A. A. Hyman, and F. Jülicher, Protein condensates as aging Maxwell fluids, *Science* **370**, 1317 (2020).
- [14] M. Linsenmeier, M. Hondele, F. Grigolato, E. Secchi, K. Weis, and P. Arosio, Dynamic arrest and aging of biomolecular condensates are modulated by low-complexity domains, RNA and biochemical activity, *Nat Commun* **13**, 3030 (2022).
- [15] M. Farag, S. R. Cohen, W. M. Borchers, A. Bremer, T. Mittag, and R. V. Pappu, Condensates formed by prion-like low-complexity domains have small-world network structures and interfaces defined by expanded conformations, *Nat Commun* **13**, 7722 (2022).
- [16] S. Ray, N. Singh, R. Kumar, K. Patel, S. Pandey, D. Datta, J. Mahato, R. Panigrahi, A. Navalkar, S. Mehra, L. Gadhe, D. Chatterjee, A. S. Sawner, S. Maiti, S. Bhatia, J. A. Gerez, A. Chowdhury, A. Kumar, R. Padinhateeri, R. Riek, G. Krishnamoorthy, and S. K. Maji, α -Synuclein aggregation nucleates through liquid–liquid phase separation, *Nat. Chem.* **12**, 705 (2020).
- [17] Y. Shen, A. Chen, W. Wang, Y. Shen, F. S. Ruggeri, S. Aime, Z. Wang, S. Qamar, J. R. Espinosa, A. Garaizar, P. St George-Hyslop, R. Collepardo-Guevara, D. A.

- Weitz, D. Vigolo, and T. P. J. Knowles, The liquid-to-solid transition of FUS is promoted by the condensate surface, *Proc Natl Acad Sci U S A* **120**, e2301366120 (2023).
- [18] S. Ranganathan and E. Shakhnovich, The physics of liquid-to-solid transitions in multi-domain protein condensates, *Biophysical Journal* **121**, 2751 (2022).
- [19] R. Takaki, L. Jawerth, M. Popović, and F. Jülicher, Theory of Rheology and Aging of Protein Condensates, *PRX Life* **1**, 013006 (2023).
- [20] A. Garaizar, J. R. Espinosa, J. A. Joseph, G. Krainer, Y. Shen, T. P. Knowles, and R. Collepardo-Guevara, Aging can transform single-component protein condensates into multiphase architectures, *Proceedings of the National Academy of Sciences* **119**, e2119800119 (2022).
- [21] G. Alberto Parada and X. Zhao, Ideal reversible polymer networks, *Soft Matter* **14**, 5186 (2018).
- [22] J. Song, N. Holten-Andersen, and G. H. McKinley, Non-Maxwellian viscoelastic stress relaxations in soft matter, *Soft Matter* **19**, 7885 (2023).
- [23] O. Lieleg, J. Kayser, G. Brambilla, L. Cipelletti, and A. R. Bausch, Slow dynamics and internal stress relaxation in bundled cytoskeletal networks, *Nature Mater* **10**, 236 (2011).
- [24] L. Berthier, Dynamic Heterogeneity in Amorphous Materials, *Physics* **4**, 42 (2011).
- [25] F. Dar, S. R. Cohen, D. M. Mitrea, A. H. Phillips, G. Nagy, W. C. Leite, C. B. Stanley, J.-M. Choi, R. W. Kriwacki, and R. V. Pappu, Biomolecular condensates form spatially inhomogeneous network fluids, *Nat Commun* **15**, 3413 (2024).
- [26] W. Götze and M. Sperl, Logarithmic relaxation in glass-forming systems, *Phys Rev E Stat Nonlin Soft Matter Phys* **66**, 011405 (2002).
- [27] D. Poland and H. A. Scheraga, Phase Transitions in One Dimension and the Helix—Coil Transition in Polyamino Acids, *The Journal of Chemical Physics* **45**, 1456 (1966).
- [28] L. M. C. Janssen, Mode-Coupling Theory of the Glass Transition: A Primer, *Frontiers in Physics* **6** (2018).
- [29] Z. W. Wu, W. Kob, W.-H. Wang, and L. Xu, Stretched and compressed exponentials in the relaxation dynamics of a metallic glass-forming melt, *Nat Commun* **9**, 5334 (2018).
- [30] W. Kob and H. C. Andersen, Testing mode-coupling theory for a supercooled binary Lennard-Jones mixture. II. Intermediate scattering function and dynamic susceptibility, *Phys. Rev. E* **52**, 4134 (1995).
- [31] J.-P. Bouchaud, Anomalous Relaxation in Complex Systems: From Stretched to Compressed Exponentials, in *Anomalous Transport* (John Wiley & Sons, Ltd, 2008) Chap. 11, pp. 327–345.
- [32] T. Wu, M. R. King, M. Farag, R. V. Pappu, and M. D. Lew, Single fluorogen imaging reveals spatial inhomogeneities within biomolecular condensates (2023).
- [33] A. Compte and J.-P. Bouchaud, Localization in one-dimensional random random walks, *J. Phys. A: Math. Gen.* **31**, 6113 (1998).
- [34] J. P. Bouchaud, Weak ergodicity breaking and aging in disordered systems, *J. Phys. I France* **2**, 1705 (1992).
- [35] E. M. Bertin and J.-P. Bouchaud, Subdiffusion and localization in the one-dimensional trap model, *Phys. Rev. E* **67**, 026128 (2003).
- [36] I. L. Morgan, R. Avinery, G. Rahamim, R. Beck, and O. A. Saleh, Glassy Dynamics and Memory Effects in an Intrinsically Disordered Protein Construct, *Phys. Rev. Lett.* **125**, 058001 (2020).
- [37] P. Sollich, F. Lequeux, P. Hébraud, and M. E. Cates, Rheology of Soft Glassy Materials, *Phys. Rev. Lett.* **78**, 2020 (1997).
- [38] H. Le Roy, J. Song, D. Lundberg, A. V. Zhukhovitskiy, J. A. Johnson, G. H. McKinley, N. Holten-Andersen, and M. Lenz, Valence can control the nonexponential viscoelastic relaxation of multivalent reversible gels, *Science Advances* **10**, ead15056 (2024).

Supplementary material
Microscopic model for glassy relaxation of condensates

Hugo Le Roy^{1,*} and Paolo De Los Rios¹

¹*Institute of Physics, École Polytechnique Fédérale de Lausanne—EPFL, 1015 Lausanne, Switzerland*

arXiv:2407.21710v1 [cond-mat.soft] 31 Jul 2024

* h.leroy@epfl.ch

S1. DERIVATION OF THE BINDING RATE

A. Polymer bound at one extremity

We first consider a Gaussian polymer of total length ℓ . By considering a conformation of the polymer as a random walk, we write the probability density that its two extremities are at \mathbf{r} from each other is given by:

$$p_{\text{Gauss}}(\mathbf{r}, \ell) = \left(\frac{3}{2\pi\ell a} \right)^{3/2} \exp\left(\frac{3\mathbf{r}^2}{2\ell a} \right) = \frac{\Omega(\mathbf{r}, \ell)}{(4\pi)^{\ell/a}}, \quad (\text{S1})$$

where $\Omega(\mathbf{r}, \ell)$ is the number of microstates for which ends are located at \mathbf{r} from one each other, while 4π is the solid angle of the random walk, and thus $(4\pi)^{\ell/a}$ is the total number of microstate associated with a free polymer. Now, considering a linker at a position \mathbf{r} , and a Gaussian polymer of length L bound at one extremity in $\mathbf{r}_0 = 0$. The probability density that a portion of the polymer located at a lineic distance ℓ from the origin of the polymer meets a sticker located in \mathbf{r} can be written as:

$$p(\mathbf{r}, \ell) = \left(\frac{3}{2\pi\ell a} \right)^{3/2} e^{-\frac{3\mathbf{r}^2}{2\ell a}} = \frac{\Omega(\mathbf{r}, \ell)}{(4\pi)^{\ell/a}} \quad (\text{S2})$$

We can write this probability density as a function of the entropy of the whole polymer:

$$S_b(\mathbf{r}, \ell) = \underbrace{\log(\Omega(\mathbf{r}, \ell))}_{\text{polymer bound at both extremities}} + \underbrace{(L - \ell) \log(4\pi)}_{\text{remaining part of the polymer}} \quad (\text{S3})$$

$$S_{ub}(\ell) = L \log(4\pi)$$

Which gives:

$$p(\mathbf{r}, \ell) = \exp(S_b(\mathbf{r}, \ell) - S_{ub}(L)) \quad (\text{S4})$$

B. Polymer bound at both extremities

Now, considering a polymer of length L bound at both its extremities in \mathbf{R}_l and \mathbf{R}_r . Following a similar reasoning as in the previous section, we write the probability that the polymer meets a sticker in \mathbf{r} , along ℓ as:

$$p(\mathbf{r}, \ell) = \frac{\Omega(\mathbf{r} - \mathbf{R}_l, \ell) \Omega(\mathbf{R}_r - \mathbf{r}, L - \ell)}{\Omega(\mathbf{R}_r - \mathbf{R}_l, L)} \quad (\text{S5})$$

$$= \left(\frac{3L}{2\pi\ell(L - \ell)} \right)^{3/2} \exp \left[-\frac{3}{2} \left(\frac{(\mathbf{R}_l - \mathbf{r})^2}{\ell a} + \frac{(\mathbf{r} - \mathbf{R}_r)^2}{(L - \ell)a} - \frac{(\mathbf{R}_r - \mathbf{R}_l)^2}{La} \right) \right]$$

Which gives a similar expression for the rates, using:

$$S_b(\mathbf{r}, l) = \log [\Omega(\mathbf{r} - \mathbf{R}_l, \ell) \Omega(\mathbf{R}_r - \mathbf{r}, L - \ell)] \quad (\text{S6})$$

$$S_{ub}(\mathbf{r}, l) = \log [\Omega(\mathbf{R}_r - \mathbf{R}_l, L)]$$

S2. DERIVATION OF THE PAIR PROBABILITY DISTRIBUTION

A. Two stickers case

Focusing on a single sticker in \mathbf{r} , with a single polymer in its vicinity. In the situation where $E_b \gg k_b T$, we assume that the stickers spend most of their time in the bound state. Starting with the master equation:

$$\partial_t p_b(\mathbf{r}, t) = k_b(\mathbf{r}, t, \ell) p_{ub}(\mathbf{r}, t) - k_{ub} p_b(\mathbf{r}, t) \quad (\text{S7})$$

$$\partial_t p_{ub}(\mathbf{r}, t) = k_{ub} p_b(\mathbf{r}, t) - k_b(\mathbf{r}, t, \ell) p_{ub}(\mathbf{r}, t) + D \nabla^2 p_{ub}(\mathbf{r}, t) \quad (\text{S8})$$

We first compute the probability that the sticker binds to the polymer along any ℓ by integrating Eq. (S2):

$$k_b(\mathbf{r}) = \int_0^L \frac{d\ell}{L} k_b(|\mathbf{r}|, \ell) = \frac{3}{2\tau_0\pi La|\mathbf{r}|} \operatorname{erfc} \left(\sqrt{\frac{3}{2aL}} |\mathbf{r}| \right), \quad (\text{S9})$$

We can now integrate Eq. (S7),(S8) over ℓ , to remove its dependency. We then define the total probability density of the linker as:

$$p(\mathbf{r}) = p_{\text{ub}}(\mathbf{r}) + p_b(\mathbf{r}) \quad (\text{S10})$$

At equilibrium, there are no diffusive, and chemical fluxes, which means that the binding / unbinding process of Eq. S7 and Eq. S8 can be equilibrated independently of the diffusion, which gives:

$$p_{\text{ub}}(\mathbf{r}) = \frac{k_{\text{ub}}}{k_b(\mathbf{r}) + k_{\text{ub}}} p(\mathbf{r}) \quad (\text{S11})$$

$$p_b(\mathbf{r}) = \frac{k_b(\mathbf{r})}{k_b(\mathbf{r}) + k_{\text{ub}}} p(\mathbf{r}) \quad (\text{S12})$$

We now sum Eq. (S7), (S8) and replace the expression of $p_{\text{ub}}(\mathbf{r})$ of Eq. S11 to obtain an equation on the total probability density of finding two stickers at a relative position \mathbf{r} from one another:

$$\partial_t p(\mathbf{r}, t) = D \nabla^2 \left[\frac{k_{\text{ub}}}{k_{\text{ub}} + k_b(\mathbf{r})} p(\mathbf{r}, t) \right] \quad (\text{S13})$$

at equilibrium, the time derivative is 0. Assuming no flux of probability at the boundary, we get:

$$\frac{k_{\text{ub}}}{k_b(\mathbf{r}) + k_{\text{ub}}} p_{\text{eq}}(\mathbf{r}) \stackrel{k_{\text{ub}} \ll k_b}{\approx} \frac{k_{\text{ub}}}{k_b(\mathbf{r})} p_{\text{eq}}(\mathbf{r}) = A \quad (\text{S14})$$

Where A is a constant. In the case of strong binding energy, we have $\forall \mathbf{r} k_b(\mathbf{r}) \gg k_{\text{ub}}$. We thus find the value of A through the following normalizing condition:

$$\int d\mathbf{r} p_{\text{eq}}(\mathbf{r}) = 1 = A \int d\mathbf{r} \frac{k_b(\mathbf{r})}{k_{\text{ub}}} = \frac{A}{k_{\text{ub}}\tau_0} \int d\mathbf{r} \underbrace{p(\mathbf{r}, \ell)}_{=1 \text{ by normalization of the Gaussian probability}} \Rightarrow A = \tau_0 k_{\text{ub}} \quad (\text{S15})$$

Thus, we find:

$$p_{\text{eq}}(\mathbf{r}) = \tau_0 k_b(\mathbf{r}) \quad (\text{S16})$$

B. N stickers case

To derive a similar probability distribution, we first integrate $p(\mathbf{r}, \ell)$ over ℓ for the case of a polymer bound at both of its extremities. To do so, we notice that $p(\mathbf{r}, \ell)$ from Eq. (S5) decay exponentially fast with the distance from each of the neighboring node. As a result, we consider that it only takes meaningful value for $\mathbf{r} \approx \mathbf{R}_l$ or $\mathbf{r} \approx \mathbf{R}_r$. In this case, we can neglect the change in entropy from the largest portion of the polymer, and write for the case $\mathbf{r} \approx \mathbf{R}_r$:

$$p(\mathbf{r}, \ell) \propto \Omega((\mathbf{r} - \mathbf{R}_l), l) \quad (\text{S17})$$

Which after computing the normalization factor, and translating the reference frame to $\mathbf{R}_\ell = 0$, gives the same formula as Eq. (S2). As a result, the attractive Casimir-like interaction between nodes becomes a simple pair interaction. We notice that the equilibrium distance distribution between stickers involves many binding-unbinding events. Consequently, we consider the average length of the polymer between two stickers to compute their interaction. Assuming that a polymer strand is spread equally between stickers, the average length between two stickers is L/N . Because the force between stickers is now a pair interaction, and because we neglected excluded volume, the distance distribution remain of the same form, and we got:

$$p_{\text{eq}}(|\mathbf{r}|) = \frac{3N}{2\pi La|\mathbf{r}|} \operatorname{erfc} \left(\sqrt{\frac{3N}{2aL}} |\mathbf{r}| \right) \quad (\text{S18})$$

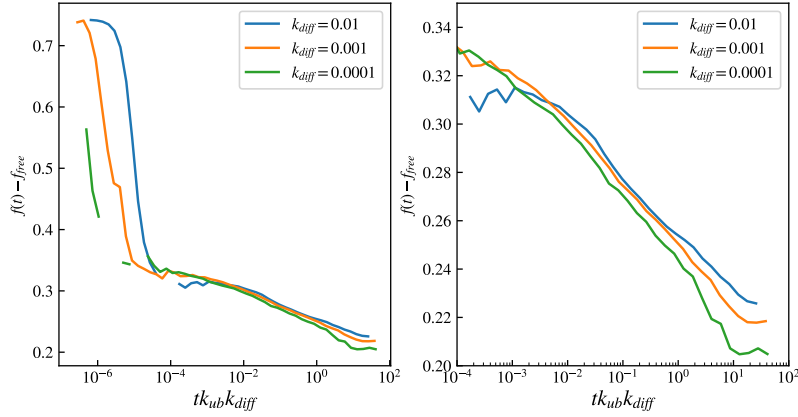


FIG. 1. Evolution of the lineic free energy difference as a function of time. on the left-hand side, we show the full relaxation process, including the early time behavior when stickers initially bind to the polymer. We cannot obtain a correct sampling of both relaxation regime at the same time, since the first one is a fast relaxation, and the second relaxation process requires a logarithmic sampling of the measurement. The time has been rescaled by the value of k_{diff} , consequently, the effective time of the first regime appear shifted as **it does not** depends on k_{diff} . On the other hand, the collapsing of the curve in the second regime highlights that the relaxation dynamic in regime is simply proportional to the value of k_{diff} . The right-hand side graph shows a zoom on the second regime, as shown in the main text.

S3. EFFECT OF k_{diff} ON THE FINAL STATE

Although we do not explicitly study the influence of the diffusion constant on the steady state free energy, we display in Fig. 1 the free energy evolution for several k_{diff} .

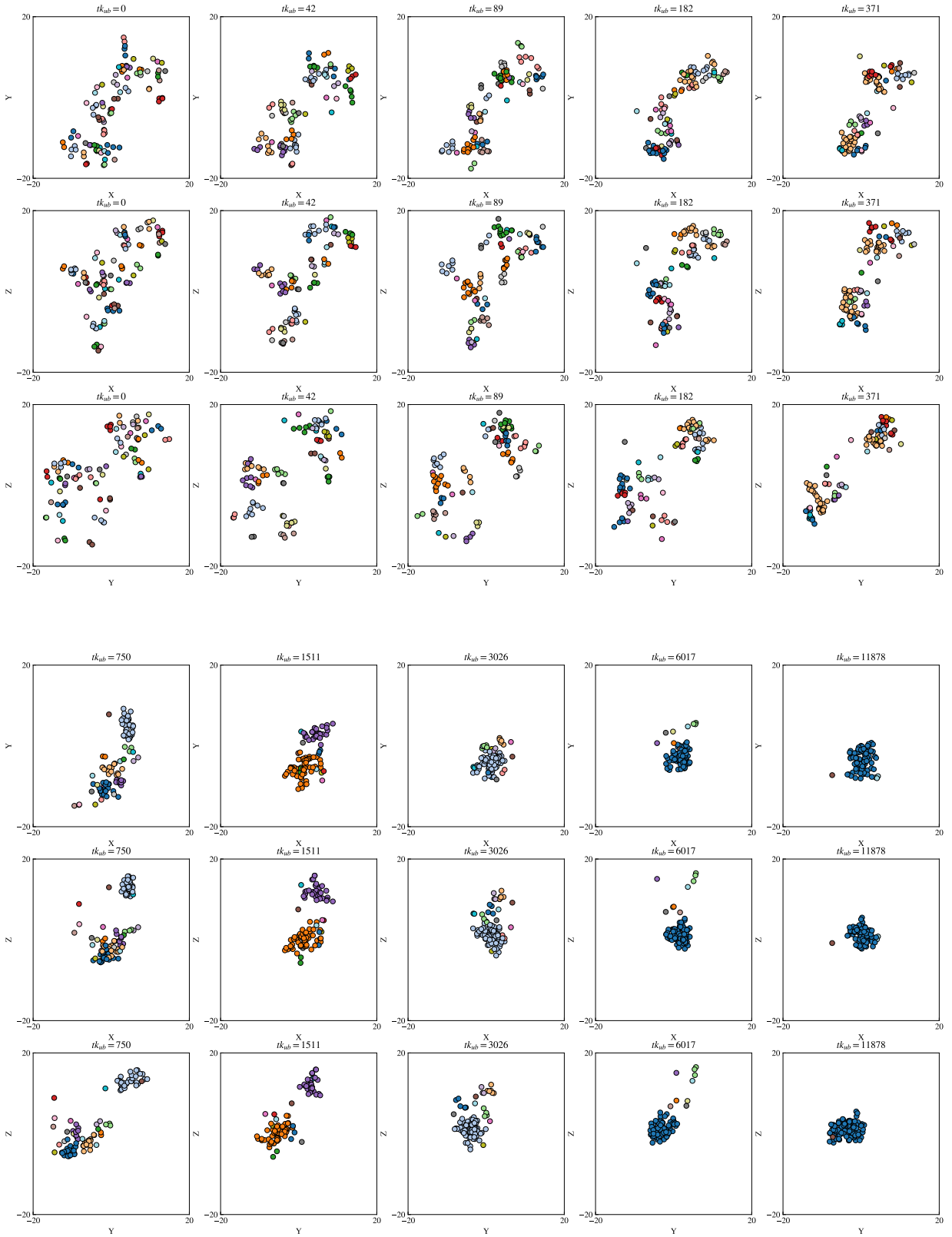


FIG. 2. Picture of the system, for $k_{\text{diff}} = 10^{-3}$, $N = 100$ stickers, and $L = 2000$ monomers. The color coding correspond to the cluster labeling, each of the three lines corresponds to a different 2D projection of the 3D system.

S4. CLUSTER DISSOLUTION TIME

Here, we adapt a similar derivation to the one of [?] chapter XII for the mean escape time. To compute the average dissolution time of a cluster, we start off of the Eq. (7) from the main text. We now look at our system as a random walker located between an absorbing boundary condition in 0, and a reflective one in N . Now considering the mean time for the random walker to reach 0, knowing that it first started in m , denoted τ_m . After a time Δt , the random walker has a probability $\omega^+ \Delta t$, $\omega^- \Delta t$ or $1 - \omega^+(m) \Delta t - \omega^-(m) \Delta t$, to respectively jump to the right, to the left, or to stay in place. Thus, we write a recursive equation for τ_m , valid $\forall m \in [1, N]$

$$\tau_m - \Delta t = \omega^-(m) \Delta t \tau_{m-1} + \omega^+(m) \Delta t \tau_{m+1} + (1 - \omega^+(m) \Delta t - \omega^-(m) \Delta t) \tau_m. \quad (\text{S19})$$

Which gives,

$$\omega^-(m)(\tau_{m-1} - \tau_m) + \omega^+(m)(\tau_{m+1} - \tau_m) = -1, \quad (\text{S20})$$

with $\tau_0 = 0$, and $\omega^-(N)(\tau_{N-1} - \tau_N) = -1$. We define:

$$\begin{aligned} \Delta_m &= \tau_{m-1} - \tau_m, \\ \tau_m &= - \sum_{\nu=1}^m \Delta_\nu \end{aligned} \quad (\text{S21})$$

which gives

$$\omega^-(m) \Delta_m - \omega^+(m) \Delta_{m+1} = -1, \quad (\text{S22})$$

with $\Delta_N = -1/\omega^-(N)$. By a recursion, we can show that $\forall \nu \in [1, N]$:

$$\Delta_\nu = - \sum_{\mu=\nu}^N \frac{\prod_{i=\nu}^{\mu-1} \omega^+(i)}{\prod_{i=\nu}^{\mu} \omega^-(i)}, \quad (\text{S23})$$

with the convention that $\prod_{i=\nu}^{\nu-1} \omega^+(i) = 1$. Using Eq. (S21), we find:

$$\tau_m = \sum_{\nu=1}^m \sum_{\mu=\nu}^N \frac{\prod_{i=\nu}^{\mu-1} \omega^+(i)}{\prod_{i=\nu}^{\mu} \omega^-(i)} \quad (\text{S24})$$

In the main text, we derived the following rates:

$$\begin{aligned} \omega^-(i) &= ik_{\text{exch}} \\ \omega^+(i) &= \bar{n}k_{\text{exch}}. \end{aligned} \quad (\text{S25})$$

In the following, we drop the indices "exch" for convenience. Injecting the expression of the rates in Eq. (S24) gives:

$$\begin{aligned} \tau_m &= \sum_{\nu=1}^m \left[\sum_{\mu=\nu+1}^N \frac{(k\bar{n})^{\mu-1-\nu}}{k^{\mu-\nu} \mu! / \nu!} + \frac{1}{k\nu} \right] \\ &= \frac{1}{k} \left[\frac{1}{\bar{n}} \sum_{\nu=1}^m \frac{\nu!}{\bar{n}^\nu} \underbrace{\sum_{\mu=\nu+1}^N \frac{\bar{n}^\mu}{\mu!}}_{S_1} + \sum_{\nu=1}^m \frac{1}{\nu} \right] \end{aligned} \quad (\text{S26})$$

For $N \rightarrow \infty$, we have:

$$S_1 = e^{\bar{n}} - \sum_{\mu=0}^{\nu} \frac{\bar{n}^\mu}{\mu!} \underset{\bar{n} \gg 1}{\sim} e^{\bar{n}} \quad (\text{S27})$$

We assume that the smaller cluster is the one that dissolve first, without knowledge on the actual smallest cluster, we assume that its size is 1.

$$\tau_1 = \frac{1}{k} \left[\frac{e^{\bar{n}}}{\bar{n}^2} + 1 \right] \underset{\bar{n} \gg 1}{\sim} \frac{e^{\bar{n}}}{k\bar{n}^2} \quad (\text{S28})$$

S5. LOGARITHMIC REGIME FOR CLUSTER GROWTH

We start from the Eq. (9) from the main text, and take the thermodynamic limit $N \gg 1$. Additionally, we assume that the number of remaining clusters is large: meaning that we are far from the plateau from Fig. 4 (b) of the main text. In this case, we have: $N/b\alpha n - 1 \sim N/\bar{n}$, and the differential equation becomes:

$$\frac{d\bar{n}}{dt} = \frac{e^{-\bar{n}}\bar{n}^3}{\tau N}. \quad (\text{S29})$$

Where we have dropped the exch for convenience. With a change of variable : $u = t/(\tau N)$, we got:

$$\frac{d\bar{n}}{du} = e^{-\bar{n}}\bar{n}^3, \quad (\text{S30})$$

which we can integrate:

$$\int_{\bar{n}=1}^{\bar{n}(t)} \frac{e^{\bar{n}'}}{\bar{n}'^3} d\bar{n}' = \int_0^{t/(\tau N)} du. \quad (\text{S31})$$

This can be computed to obtain:

$$e - \text{Ei}(1) - \left[\frac{e^{\bar{n}(t)}(1 + \bar{n}(t))}{\bar{n}(t)^2} - \text{Ei}(\bar{n}(t)) \right] = \frac{t}{\tau N}, \quad (\text{S32})$$

where Ei is the exponential integral function defined as:

$$\text{Ei}(x) = \int_{-\infty}^x \frac{e^t}{t} dt. \quad (\text{S33})$$

From the asymptotic series of the exponential integral, we get:

$$\text{Ei}(x) = \frac{e^x}{x} \left(1 + O\left(\frac{1}{x}\right) \right), \quad (\text{S34})$$

thus, for x large, we write the left-hand side of Eq. (S32) as:

$$e - \text{Ei}(1) - \left[\frac{e^{\bar{n}(t)}(1 + \bar{n}(t))}{\bar{n}(t)^2} - \text{Ei}(\bar{n}(t)) \right] \underset{\bar{n} \gg 1}{\sim} \frac{e^{\bar{n}(t)}}{\bar{n}(t)}, \quad (\text{S35})$$

which we plug into Eq. (S32) to obtain:

$$\frac{e^{\bar{n}(t)}}{\bar{n}(t)} \sim \frac{t}{\tau N}. \quad (\text{S36})$$

For large \bar{n} , the left-hand side behaves like an exponential and we find:

$$\bar{n}(t) \propto \log(t). \quad (\text{S37})$$